

Nonlinear spherical Alfvén waves

Ulf Torkelsson,¹ G. Christopher Boynton,²

¹*Institute of Astronomy, Madingley Road, Cambridge CB3 0HA, United Kingdom*

²*Physics Department, Univ. of Miami, P. O. Box 248046, Coral Gables, FL 33124, USA*

2 October 2018

ABSTRACT

We present an one-dimensional numerical study of Alfvén waves propagating along a radial magnetic field. Neglecting losses, any spherical Alfvén wave, no matter how small its initial amplitude is, becomes nonlinear at sufficiently large radii. From previous simulations of Alfvén waves in plane parallel atmospheres we did expect the waves to steepen and produce current sheets in the nonlinear regime, which was confirmed by our new calculations. On the other hand we did find that even the least nonlinear waves were damped out almost completely before $10 R_{\odot}$. A damping of that kind is required by models of Alfvén wave-driven winds from old low-mass stars as these winds are mainly accelerated within a few stellar radii.

Key words: MHD – waves – solar wind – stars: mass-loss

1 INTRODUCTION

Spherically symmetric models are often the simplest realistic models conceivable for astrophysical systems, and have been applied successfully to describe not only hydrostatic objects such as stars, but also hydrodynamic processes, for instance stellar winds (Parker 1958). In many cases it is desirable to extend a spherically symmetric hydrodynamic problem to the analogous magnetohydrodynamic problem. In a global sense such a magnetohydrodynamic analogue cannot exist, as that would require the existence of magnetic monopoles. Locally, however, the magnetic field is divergence-free, and presents a natural approximation of a region with a diverging magnetic field. In hydrodynamics there are only acoustic waves (for spherical sound waves see e.g. Landau & Lifshitz 1987), but the magnetic field introduces Alfvén waves. These transverse magnetic field oscillations cannot be extended to cover an entire spherical surface without introducing discontinuities, but once again it will not present any difficulties locally.

In a previous paper (Boynton & Torkelsson 1996, hereafter Paper 1) we have shown that nonlinear Alfvén waves in a planar geometry can steepen and form current sheets, and thereby be damped by Joule dissipation or by doing mechanical work on the background medium. The efficiency of this mechanism is limited by the Alfvén wave becoming less nonlinear as it propagates upwards through a stratified medium. A spherical Alfvén wave on the other hand may become less nonlinear for some time, but eventually has to grow nonlinear again because of the divergence of the background magnetic field. Furthermore the gas pressure decreases faster than the magnetic pressure with height independently of whether the symmetry is plane-parallel or

spherical, so that the Alfvén wave becomes more dynamically important. Models of Alfvén wave-driven outflows have been constructed by Hartmann & MacGregor (1980, 1982) to explain the winds from late-type giants, although a more popular model is that the outflows are driven by radiation pressure working on dust in the stellar atmosphere. It has been pointed out that the Alfvén waves must damp within a few stellar radii to avoid accelerating the wind to too high velocities. There is no generally accepted model for this damping and Holzer, Flå & Leer (1983) have pointed out that the stellar wind depends sensitively on the damping mechanism.

A spherically symmetric model may also apply to the coronal holes observed on the Sun (Bohlin 1976, Zirker 1977). The magnetic field in a coronal hole is open, which allows the plasma to expand outwards and form the so-called fast solar wind. This component of the solar wind is too fast to be described by the classical Parker (1958) model, and it is possible that the extra acceleration is provided by Alfvén waves. Alfvén waves have been observed further out in the solar wind (Belcher & Davis 1971, Balogh et al. 1995), but it is not known how these waves relate to the ones that are supposedly present in the corona.

Section 2 describes the initial hydrostatic model and summarizes the properties of linear waves propagating through it. The results of our numerical simulations are presented in Sect. 3. Section 4 discusses the physical interpretation and the astrophysical consequences of our results, in particular, with respect to solar and stellar winds, and our conclusions are summarized in Sect. 5.

2 THE STATIC MODEL AND ITS WAVE MODES

2.1 The static model

We assume a spherically symmetric Sun-like star. On top of the stellar surface there is an isothermal corona at a temperature of 10^6 K. For a corona in hydrostatic equilibrium the density can be written as

$$\rho_0(z) = \rho_0(0) \exp\left(-\frac{R}{H} \frac{z}{R+z}\right), \quad (1)$$

where $\rho_0(0)$ is the coronal density at the stellar surface, R is the stellar radius, z the height above the stellar surface and $H = 2k_B T R^2 / (G M m_H) = 6.1 \cdot 10^7$ m, a scale height, with k_B Boltzmann's constant, T the temperature, G the gravitational constant, M the mass of the star, and m_H the mass of a hydrogen atom. Throughout this paper subscript 0s, with a few obvious exceptions, refer to the undisturbed background and 0s as arguments to functions mean the functional values at $z = 0$, that is the stellar surface. The isothermal sound speed, c_s , which is what matters as we are assuming isothermality in the dynamical model, is $1.3 \cdot 10^5$ m s $^{-1}$ and $\rho_0(0)$ is put to $5 \cdot 10^{-13}$ kg m $^{-3}$. A vertical magnetic field, $B_z(z) \propto (R+z)^{-2}$, gives an Alfvén speed, $v_A = B_z / \sqrt{\mu_0 \rho}$, with the z -dependence of Fig. 1a. For $B_z(0) = 3 \cdot 10^{-4}$ T, the Alfvén wave is supersonic even at $z = 14 R_\odot$, whereas for $B_z(0) = 10^{-5}$ T the Alfvén wave is subsonic everywhere. Assuming a period of 300 s the wavelength is always small compared to the scale height (Fig. 1b), except for $B_z(0) = 3 \cdot 10^{-4}$ T when it exceeds the scale height for $z < 2R_\odot$ and is comparable to the solar radius at $z \approx 1.5R_\odot$. Note that for $B_z(0) = 10^{-5}$ T we choose a period of 900 s, to get the same wavelength as for $B_z(0) = 3 \cdot 10^{-5}$ T.

2.2 Linear theory of spherical waves

The magnetohydrodynamic equations for a spherically symmetric system can be written as

$$\frac{\partial \rho}{\partial t} + \frac{1}{(R+z)^2} \frac{\partial}{\partial z} [(R+z)^2 \rho v_z] = 0, \quad (2)$$

$$\frac{\partial}{\partial t} (\rho v_x) + \frac{1}{(R+z)^2} \frac{\partial}{\partial z} [(R+z)^2 \rho v_x v_z] = B_z J_y - \rho \frac{v_x v_z}{R+z}, \quad (3)$$

$$\frac{\partial}{\partial t} (\rho v_y) + \frac{1}{(R+z)^2} \frac{\partial}{\partial z} [(R+z)^2 \rho v_y v_z] = -B_z J_x - \rho \frac{v_y v_z}{R+z}, \quad (4)$$

$$\frac{\partial}{\partial t} (\rho v_z) + \frac{1}{(R+z)^2} \frac{\partial}{\partial z} [(R+z)^2 \rho v_z^2] = -\frac{\partial p}{\partial z} - B_x J_y + B_y J_x - \rho g + \rho \frac{v_x^2 + v_y^2}{R+z}, \quad (5)$$

$$\frac{\partial B_x}{\partial t} + \frac{1}{R+z} \frac{\partial}{\partial z} [(R+z) B_x v_z] = \frac{1}{R+z} \frac{\partial}{\partial z} [(R+z) B_z v_x], \quad (6)$$

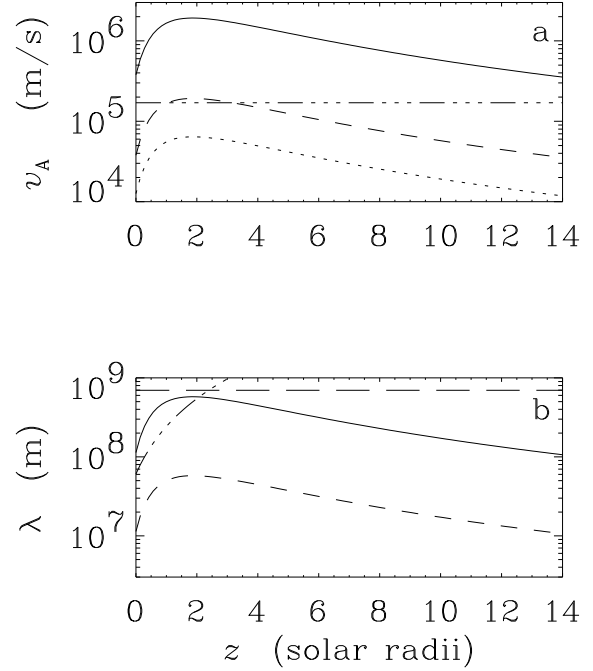


Figure 1. (a) Alfvén velocity as a function of height, z , for magnetic field strengths of $3 \cdot 10^{-4}$ T (solid line), $3 \cdot 10^{-5}$ T (dashed line) and $1 \cdot 10^{-5}$ T (dotted line) as measured at $z = 0$. The sound speed is plotted as a dash-dotted line. (b) The wavelength of an Alfvén wave with a period of 300 s as a function of z for the same magnetic field strengths. We do not plot the wavelength for $1 \cdot 10^{-5}$ T, as its period of 900 s gives it the same wavelength as $3 \cdot 10^{-5}$ T with a period of 300 s. The dash-dotted line denotes the local pressure scale height and the long-dashed line the solar radius

$$\frac{\partial B_y}{\partial t} + \frac{1}{R+z} \frac{\partial}{\partial z} [(R+z) B_y v_z] = \frac{1}{R+z} \frac{\partial}{\partial z} [(R+z) B_z v_y], \quad (7)$$

where ρ , v_x , v_y , B_x and B_y stand for the density and the transverse components of the velocity and the magnetic field. v_z is the velocity along the background magnetic field, g the gravitational field strength, and $p = c_s^2 \rho$ is the pressure. The need for an energy equation is eliminated by assuming all processes to be isothermal, and B_z must be independent of time to keep the magnetic field divergence-free. The electric current density is given by

$$J_x = -\frac{1}{\mu_0} \frac{1}{R+z} \frac{\partial}{\partial z} [(R+z) B_y], \quad (8)$$

and

$$J_y = \frac{1}{\mu_0} \frac{1}{R+z} \frac{\partial}{\partial z} [(R+z) B_x], \quad (9)$$

where μ_0 is the permeability of free space.

We linearize the equations around a, possibly, stratified static background medium and a radial magnetic field $B_z = B_z(0) \left(\frac{R}{R+z}\right)^2$. For brevity we leave out the y -components, and use $r = R + z$.

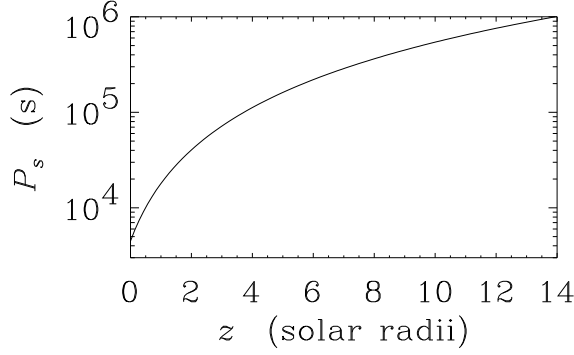


Figure 2. The maximal period for acoustic waves in a stratified atmosphere, P_s , as a function of z

$$\frac{\partial \tilde{\rho}}{\partial t} + \frac{1}{r^2} \frac{\partial}{\partial r} (r^2 \rho_0 v_z) = 0, \quad (10)$$

$$\frac{\partial}{\partial t} (\rho_0 v_x) = B_z(0) \left(\frac{R}{r} \right)^2 \frac{1}{\mu_0} \frac{1}{r} \frac{\partial}{\partial r} (r B_x), \quad (11)$$

$$\frac{\partial}{\partial t} (\rho_0 v_z) = -c_s^2 \frac{\partial \tilde{\rho}}{\partial r} - \tilde{\rho} g, \quad (12)$$

$$\frac{\partial B_x}{\partial t} = \frac{1}{r} \frac{\partial}{\partial r} \left(r B_z(0) \left(\frac{R}{r} \right)^2 v_x \right), \quad (13)$$

where we have written the density as $\rho = \rho_0 + \tilde{\rho}$. These equations separate into two groups, Eqs. (10) and (12) describing acoustic waves, and Eqs. (11) and (13) describing Alfvén waves.

As a first example we assume that ρ_0 is constant and $g = 0$. The acoustic waves are then described by two wave equations

$$\frac{\partial^2 \tilde{\rho}}{\partial t^2} = c_s^2 \frac{1}{r^2} \frac{\partial}{\partial r} \left(r^2 \frac{\partial \tilde{\rho}}{\partial r} \right), \quad (14)$$

and

$$\frac{\partial^2 v_z}{\partial t^2} = c_s^2 \frac{\partial}{\partial r} \left[\frac{1}{r^2} \frac{\partial}{\partial r} (r^2 v_z) \right], \quad (15)$$

which have the solutions

$$\tilde{\rho} = \tilde{\rho}(0) \frac{R}{r} e^{i(kr - \omega t)}, \quad (16)$$

where $\tilde{\rho}(0)$ is the amplitude of the density fluctuations at $r = R$ and

$$v_z = \omega \frac{\tilde{\rho}(0)}{\rho_0} R \frac{\partial}{\partial r} \left(\frac{e^{i(kr - \omega t)}}{ik^2 r} \right) \quad (17)$$

with the dispersion relation

$$\omega^2 = c_s^2 k^2 \quad (18)$$

(cf. Landau & Lifshitz 1987, Ch. 70).

In the case of a stratified medium the wave equation for the sound waves can be written as

$$\frac{\partial^2 \tilde{\rho}}{\partial t^2} = \frac{c_s^2}{r^2} \frac{\partial}{\partial r} \left(r^2 \frac{\partial \tilde{\rho}}{\partial r} \right) + g \frac{\partial \tilde{\rho}}{\partial r}. \quad (19)$$

For $g = GM/r^2$ the background density is $\propto \exp(-\frac{R}{H} \frac{z}{R+z})$, where H is the scale height at $z = 0$. We write the density fluctuations as

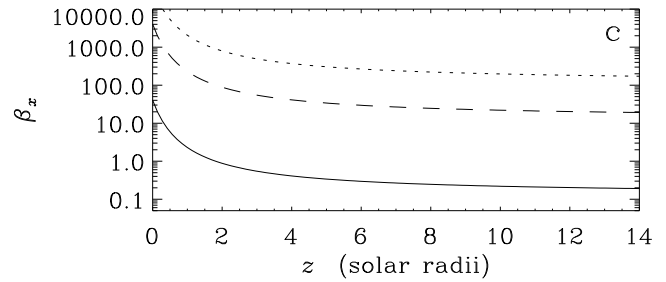
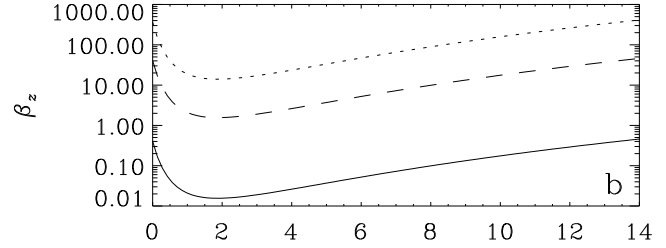
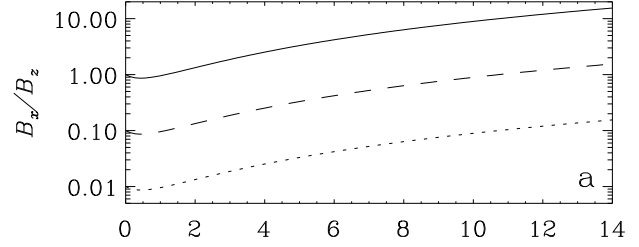


Figure 3. (a) The relative amplitude of an Alfvén wave propagating through a stratified atmosphere. The solid, dashed and dotted lines represent waves of initial relative amplitudes of 1, 0.1 and 0.01, respectively. (b, c) The ratio of gas to magnetic pressure for the background field, B_z (b) and the oscillating field B_x (c). B_z is $3 \cdot 10^{-4}$ T (solid line), $3 \cdot 10^{-5}$ T (dashed line), and 10^{-5} T dotted line. The relative amplitude of the oscillations is $B_x(0)/B_z(0) = 0.1$

$$\tilde{\rho} = \tilde{\rho}(0) \frac{R}{r} \exp \left(-\frac{R}{2H} \frac{z}{R+z} \right) e^{i(kz - \omega t)} \quad (20)$$

(cf. Paper 1). The resulting dispersion relation is

$$\omega^2 = c_s^2 k^2 + \frac{c_s^2 R^4}{4H^2 r^4}, \quad (21)$$

implying that acoustic waves with frequencies $\omega < N_s = c_s R^2 / (2Hr^2)$ are evanescent (cf. Lamb 1908, 1932). We plot the corresponding period, $P_s = 2\pi/N_s$ in Fig. 2.

Equations (11) and (13) can be rewritten as (cf. Heinemann & Olbert 1980, Leer, Holzer & Flå 1982, MacGregor & Charbonneau 1994)

$$\frac{\partial f}{\partial t} = v_A(0) \left(\frac{R}{r} \right)^2 \left(\frac{g}{r} - \frac{\partial f}{\partial r} \right), \quad (22)$$

and

$$\frac{\partial g}{\partial t} = v_A(0) \left(\frac{R}{r} \right)^2 \left(-\frac{f}{r} + \frac{\partial g}{\partial r} \right), \quad (23)$$

Table 1. Simulations of linearly polarized Alfvén waves with period, P , travelling through an isothermal medium stratified according to Eq. (1) with a base density $5 \cdot 10^{-13} \text{ kg m}^{-3}$ and a background magnetic field, B_z , decreasing as $1/(R+z)^2$. The temperature of the medium is 10^6 K , which corresponds to a sound speed of $1.29 \cdot 10^5 \text{ m s}^{-1}$. The computational domain covers the the corona between 1 and $15 R_\odot$ outside of a solarlike star for Models 1a - 1c, and between 1 and $16 R_\odot$ for Models 2a - 3c. The homogeneous (H) models are similar but has a constant density of $10^{-14} \text{ kg m}^{-3}$, their radial extents are $0.15 R_\odot$ (H1a-H1c), $0.3 R_\odot$ (H1d) and $0.6 R_\odot$ (H2a-H2c) with the lower boundary at $1 R_\odot$. The driven Alfvén wave is polarized at 45° to the x -axes for all of the simulations. Δt denotes the time step and N the number of spatial grid points used in the respective models. $B_z(0)$ is the strength of the background magnetic field, $v_A(0)$ the Alfvén velocity, $(B_{\text{osc}}/B_z)(0)$ the relative amplitude of the Alfvén wave and $\beta_{\text{mag}}(0)$ the plasma beta all calculated at $z = 0$

Model	Δt (s)	N	$B_z(0)$ (T)	P (s)	$v_A(0)$ (m s^{-1})	$(B_{\text{osc}}/B_z)(0)$	$\beta_{\text{mag}}(0)$
H1a	0.25	720	$5 \cdot 10^{-6}$	300	$4.4 \cdot 10^4$	0.01	17
H1b	0.25	720	$5 \cdot 10^{-6}$	300	$4.4 \cdot 10^4$	0.1	17
H1c	0.25	720	$5 \cdot 10^{-6}$	300	$4.4 \cdot 10^4$	1.0	17
H1d	0.25	1440	$5 \cdot 10^{-6}$	300	$4.4 \cdot 10^4$	1.0	17
H2a	1	720	$2 \cdot 10^{-5}$	300	$1.8 \cdot 10^5$	0.01	1.0
H2b	1	720	$2 \cdot 10^{-5}$	300	$1.8 \cdot 10^5$	0.1	1.0
H2c	1	720	$2 \cdot 10^{-5}$	300	$1.8 \cdot 10^5$	1.0	1.0
1a	1	15120	$1 \cdot 10^{-5}$	900	$1.3 \cdot 10^4$	0.01	210
1b	1	15120	$1 \cdot 10^{-5}$	900	$1.3 \cdot 10^4$	0.1	210
1c	1	15120	$1 \cdot 10^{-5}$	900	$1.3 \cdot 10^4$	1.0	210
2a	1	15120	$3 \cdot 10^{-5}$	300	$3.8 \cdot 10^4$	0.01	23
2b	1	15120	$3 \cdot 10^{-5}$	300	$3.8 \cdot 10^4$	0.1	23
2c	1	15120	$3 \cdot 10^{-5}$	300	$3.8 \cdot 10^4$	1.0	23
3a	0.25	7560	$3 \cdot 10^{-4}$	300	$3.8 \cdot 10^5$	0.01	0.23
3b	0.25	7560	$3 \cdot 10^{-4}$	300	$3.8 \cdot 10^5$	0.1	0.23
3c	0.25	7560	$3 \cdot 10^{-4}$	300	$3.8 \cdot 10^5$	1.0	0.23

where

$$f = v_x - \frac{B_x}{\sqrt{\mu_0 \rho_0}}, \quad g = v_x + \frac{B_x}{\sqrt{\mu_0 \rho_0}}, \quad (24)$$

and $v_A(0) = B_z(0)/\sqrt{\mu_0 \rho_0(0)}$ is the Alfvén velocity at $r = R$, so that

$$v_x = \frac{1}{2}(f + g) \quad (25)$$

and

$$B_x = \frac{1}{2}\sqrt{\mu_0 \rho_0}(-f + g). \quad (26)$$

Note that $f = 0$ and $g = 0$ yield waves propagating downwards and upwards, respectively. Substituting $f(r, t) = F(r)e^{-i\omega t}$ and $g(r, t) = G(r)e^{-i\omega t}$ we get

$$\frac{d}{dr} \begin{pmatrix} F \\ G \end{pmatrix} = \begin{pmatrix} \frac{i\omega}{v_A} \left(\frac{r}{R}\right)^2 & \frac{1}{r} \\ \frac{1}{r} & -\frac{i\omega}{v_A} \left(\frac{r}{R}\right)^2 \end{pmatrix} \begin{pmatrix} F \\ G \end{pmatrix} \quad (27)$$

The general solution to these equations is rather complicated, and we will restrict ourselves to cite some general and useful results, that can be derived from simple physical arguments.

First we derive the scaling properties of the amplitudes of v_x and B_x in the WKB sense. Consider the Poynting flux

$$\mathbf{S} = \frac{\mathbf{E} \times \mathbf{B}}{\mu_0}, \quad (28)$$

with the electric field, $\mathbf{E} = -\mathbf{v} \times \mathbf{B} + \mathbf{J}/\sigma$, where we assume that the conductivity, σ , is infinite. If there are no losses, the amplitude of the radial component of the Poynting vector S_z will be proportional to $1/r^2$. S_z is also proportional

to $B_z B_x v_x$, the oscillating transverse magnetic and velocity fields, and as $B_z \propto 1/r^2$ in our monopole geometry, $B_x v_x$ is not explicitly dependent upon r . The oscillating magnetic and velocity fields of an outgoing Alfvén wave are related by

$$v_x = -\frac{B_x}{\sqrt{\mu_0 \rho_0}}, \quad (29)$$

which gives $B_x \propto \rho_0^{1/4}$ and $v_x \propto \rho_0^{-1/4}$. We plot the relative amplitude of the Alfvén wave, B_x/B_z , in Fig. 3a. In Figs. 3b and c we compare B_z and B_x , respectively, to the gas pressure by calculating the magnetic beta $\beta_{x,z} = 2\mu_0 p(z)/B_{x,z}^2$.

The main effect of the deviations from the WKB-approximation is that the waves can be reflected against gradients in the Alfvén speed. This problem has been discussed for linearized spherical Alfvén waves by An et al. (1990) and Lou & Rosner (1994). The reflection is important as it increases the momentum transferred from the Alfvén wave to the medium.

3 RESULTS OF THE NUMERICAL SIMULATIONS

We modified the code of Paper 1 to simulate Alfvén waves in a spherically symmetric magnetic field. In addition we now solve for both transverse components of the velocity and magnetic fields, so that also circularly polarized waves can be described. In general our waves are linearly polarized at 45° to the x -axis. Initial test runs showed that the boundary conditions from Paper 1 were too reflective at the upper boundary. After some experiments we found that a satisfactory solution was to extrapolate the boundary val-

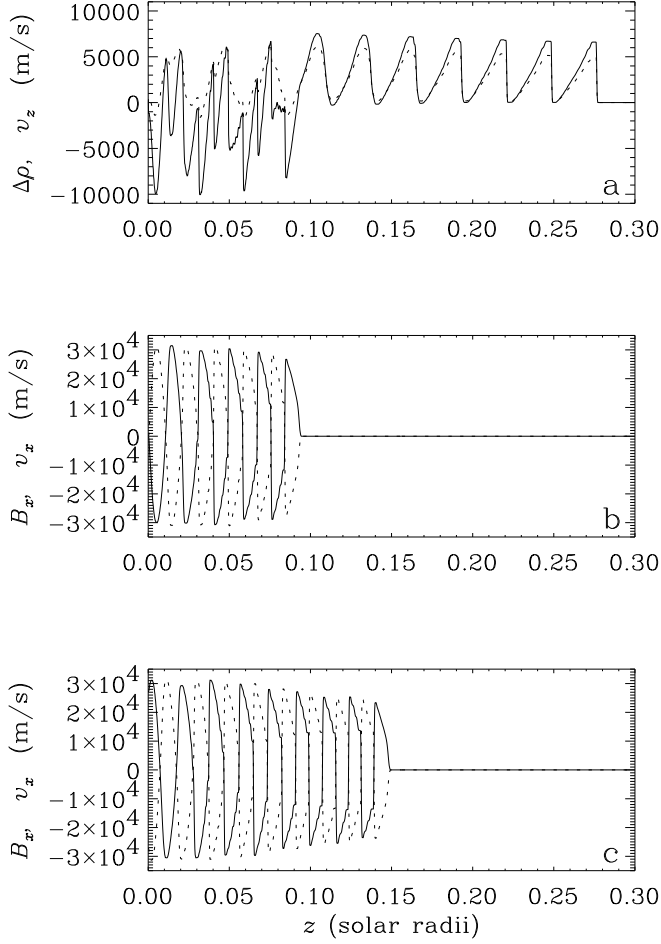


Figure 4. Magnetohydrodynamic waves propagating in a spherically symmetric magnetic field with a uniform background density (Model H1d). (a) $\Delta\rho$ (solid line), and v_z (dotted line) oscillations at 6000 s. Both quantities are measured in velocity units. The lower two panels show B_x (solid line) and v_x (dotted line) oscillations at (b) 6000 s and (c) 10000 s, respectively, both measured in velocity units. (a) shows the acoustic precursor ($z > 0.1R_\odot$) to the Alfvén wave in (b), and the oscillations generated by the magnetic pressure ($z < 0.1R_\odot$). The Alfvén wave is gradually damped as it steepens into current sheets (c)

ues of ρv_z , B_x and B_y from the last three grid points, and calculate ρv_x and ρv_y from the requirement that they should describe Alfvén waves propagating out through the boundary. The boundary conditions at the lower boundary are the same as in Paper 1, that is we drive an upwards propagating Alfvén wave, and keep all other variables fixed at their initial values.

Table 1 describes the models that we have calculated. The H-models are homogeneous in the sense that they have constant density and temperature, and no gravity, but the magnetic field still goes as $1/(R+z)^2$.

3.1 Wave propagation

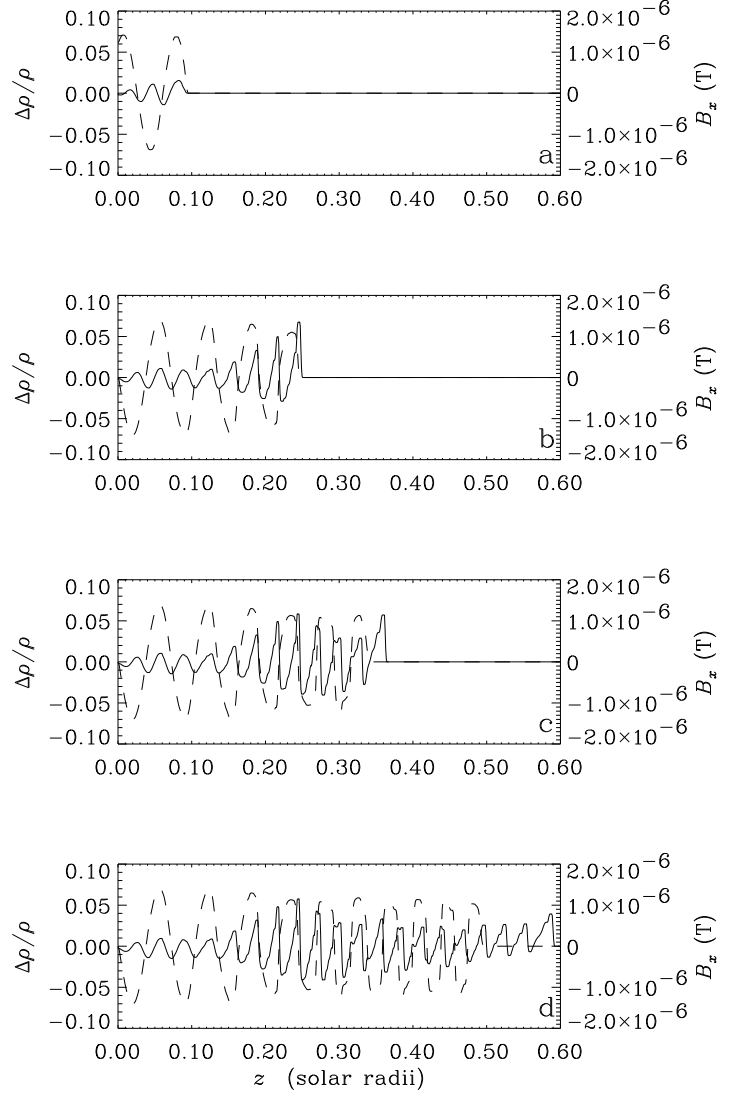


Figure 5. Magnetohydrodynamic waves propagating in a spherically symmetric magnetic field with a uniform background density (Model H2b). The left axis and the solid line show $\Delta\rho/\rho_0$ and the right axis and the dotted line B_z . The times are (a) 400 s, (b) 1200 s, (c) 1800 s, and (d) 3000 s, respectively. At the start the Alfvén wave is propagating faster than a sound wave so that in (a) we see density oscillations carried by the magnetic field, but as the Alfvén velocity decreases there is a sound wave that overtakes the Alfvén wave (b-d)

Table 2. The maximum of the precursory density fluctuations $(\Delta\rho/\rho_0)_{1\max}$ and of the second-order fluctuations $(\Delta\rho/\rho_0)_{2\min}$ in the interacting Alfvén and acoustic waves for Models H1a-H1c

$(B_{\text{osc}}/B_z)(0)$	$(\Delta\rho/\rho_0)_{1\max}$	$(\Delta\rho/\rho_0)_{2\min}$
0.01	$4.8 \cdot 10^{-6}$	$-6 \cdot 10^{-6}$
0.1	$4.8 \cdot 10^{-4}$	$-6 \cdot 10^{-4}$
1.0	$4.7 \cdot 10^{-2}$	$-6 \cdot 10^{-2}$

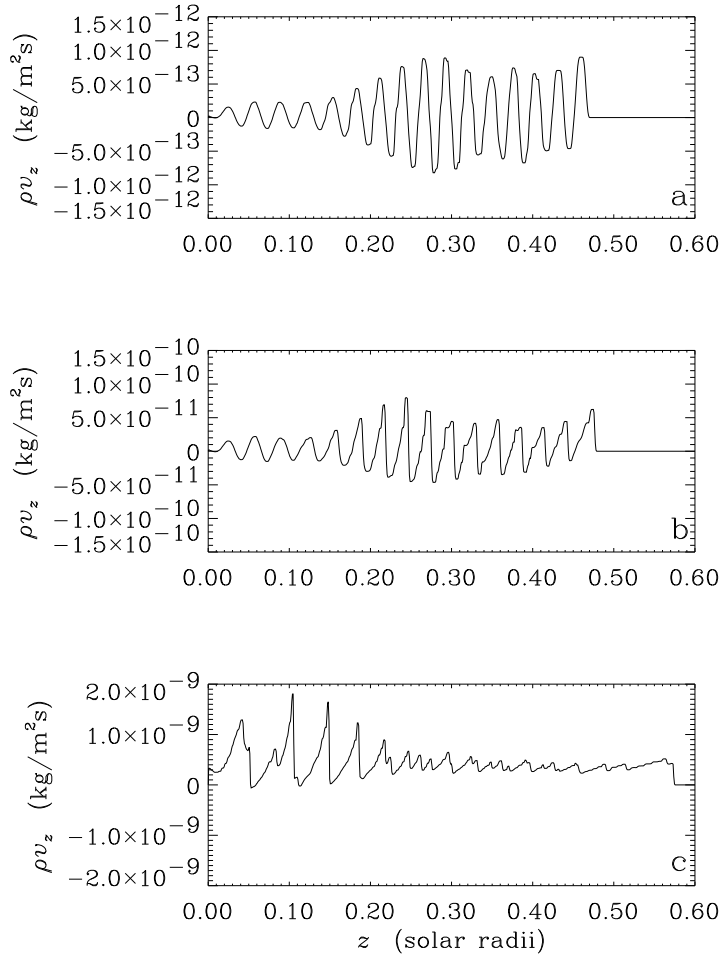


Figure 6. ρv_z as a function of z for Models H2a - c (a - c) at 2400 s. Note how ρv_z changes character from being a propagating wave (a,b) to an outflow (c) when the amplitude of the Alfvén wave increases

3.1.1 Unstratified models

The amplitudes of the transverse velocities and magnetic fields are not affected by the divergence of the radial magnetic field, but they are affected by the stratification in the same way as in the plane-parallel case considered in Paper 1. The most straightforward cases are obviously the ones without stratification, where the Alfvén velocity decreases as $1/(R+z)^2$. Models H1a-d are particularly simple as $v_A < c_s$ everywhere in these models, so that the Alfvén wave has an acoustic precursor. For high amplitude waves, such as H1c and H1d, both the acoustic precursor and the Alfvén wave steepen to form shocks and current sheets, respectively (Fig. 4). Note that we have transformed the density, $\Delta\rho = \rho - \rho_0$, and magnetic field, B_x , oscillations to velocities by multiplying with c_s/ρ_0 and $1/\sqrt{\mu_0\rho_0}$, respectively. We quantify the amplitude of the precursor by defining $(\frac{\Delta\rho}{\rho_0})_{1\max}$ as the maximum of the density fluctuations in the acoustic precursor (the density does not drop below its background value). Likewise we call the minimum of the density fluctuations inside the Alfvén wave $(\frac{\Delta\rho}{\rho_0})_{2\min}$. The numerical values for these quantities are given in Tab. 2 for Models H1a - H1c.

Both the precursors and the density fluctuations inside the Alfvén wave are proportional to the square of the amplitude of the Alfvén wave. This is natural as they are produced by the magnetic pressure of the Alfvén wave.

The situation is more complicated in Models H2a-c, where $v_A > c_s$ at $z = 0$, but $c_s > v_A$ for $z > 0.04R_\odot$. The acoustic wave lags behind the Alfvén wave at first. The density oscillations propagating with the Alfvén wave in Fig 5a are not acoustic waves, but rather ρ and v_z oscillations caused by the magnetic pressure oscillations (cf. Hollweg 1971). Density maxima occur initially where there is a maximum in the magnetic pressure, but drift out of phase when the acoustic wave overtakes the Alfvén wave (Fig. 5b,c). The density fluctuations simultaneously increase in amplitude, and eventually steepen into shocks and lose energy (Fig. 5d). It is instructive to study these oscillations as a function of the amplitude of the Alfvén waves. For a low amplitude Alfvén wave the density fluctuations are essentially a propagating wave which does not transport any significant amount of mass (Fig. 6a). This wave is growing in amplitude up to $z = 0.3R_\odot$ after which it remains constant or even decreases in amplitude again (Fig. 6b). The amplitude of the wave is varying roughly as the square of the amplitude of the Alfvén wave as can be found by comparing Figs. 6a and b, and it is propagating at the sound speed, $1.3 \cdot 10^5 \text{ m s}^{-1}$. ρv_z changes character completely for a nonlinear Alfvén wave (Fig. 6c). There is an outflow of mass, which is concentrated to shocks that are separated in time by roughly half the period of the Alfvén wave. The front of the outflow is initially propagating at $2 \cdot 10^5 \text{ m s}^{-1}$, but slows down to $1.5 \cdot 10^5 \text{ m s}^{-1}$, at 3000 s, which is still supersonic. However the outflow velocity, v_z , is mainly subsonic, although it may reach peak values as high as $1.4 \cdot 10^5 \text{ m s}^{-1}$.

3.1.2 Stratified models

The stratified models are different with respect to the Alfvén velocity in the sense that v_A first increases with z , but starts to decrease again above $z = 2R_\odot$. Models 1a-c have $v_A < c_s$ everywhere, so that we expect to see an acoustic precursor. We increased the period to 900 s for these models, as a shorter wavelength would have required a finer resolution, and thus more CPU time. We show snapshots of Models 1b and c in Fig. 7. Figure 7d shows clear signs of the nonlinear damping beyond $z = 1R_\odot$ as v_x stops increasing in amplitude. The front of the Alfvén wave has advanced further in Fig. 7d than 7b, which is surprising as both snapshots are taken after the same simulation time. It is the wave in Fig. 7b that is propagating at the expected Alfvén speed, whereas the nonlinear Alfvén wave is propagating too fast (see Sect. 4.2).

Models 2a-2c are more interesting because the Alfvén speed is comparable to the sound speed in the interval $1R_\odot \leq z \leq 3R_\odot$. The most striking feature in the early stages of Model 2b is however unrelated to this. Figure 8 shows how the acoustic oscillations described by ρv_z grow in amplitude, but reach a maximum at $z = 0.7$. After this the sound waves steepen and dissipate the momentum that they are carrying (Fig. 8d). At 50 000 s we see that the amplitude of the Alfvén wave decreases sharply between $z = 3R_\odot$ and $z = 5R_\odot$ (Fig. 9b). There are also signs of oscillations at higher frequencies superposed on the wave, in particular

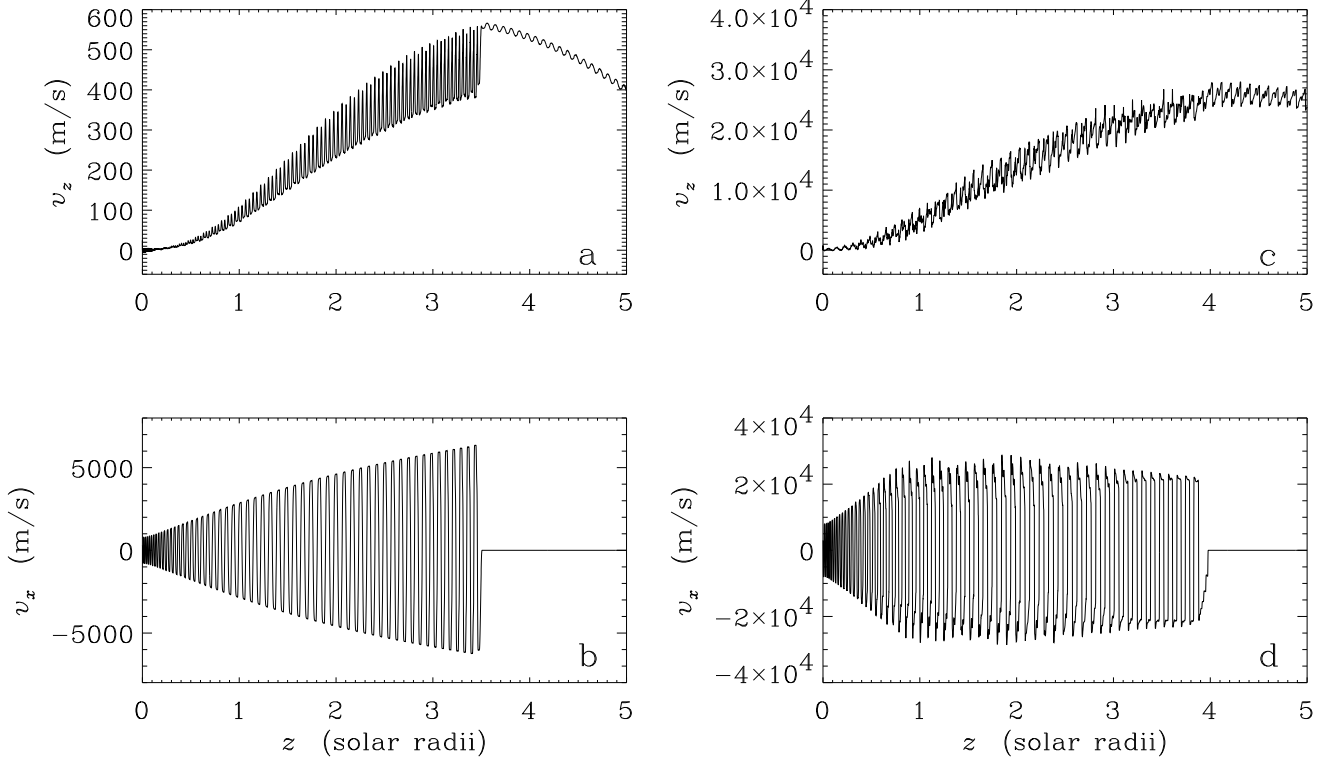


Figure 7. v_z and v_x at 50 000 s for Models 1b (a) and (b), and 1c (c) and (d). (a, b) show an Alfvén wave of low amplitude with an acoustic precursor. At higher amplitude (c, d) the Alfvén wave is strongly damped by nonlinear steepening, and the Alfvén wave front is propagating faster

downward of $z = 5R_\odot$, and a general low-frequency modulation at $z < 1R_\odot$. Fig. 9c suggests that the first 7 or so wavelengths of the wave are less damped and show less extraneous oscillations than the following wavelengths. The same effects are present in Model 2c too, but in addition the wavefront of Model 2c is propagating super-Alfvénically, which we will try to explain in Sect. 4.2. Model 2c crashed eventually as the magnetic pressure evacuated a part of the grid, which was expected as the pressure of the oscillatory magnetic field is comparable to the gas pressure.

The only one of Models 3 that has got $(B_x^2 + B_y^2)/(2\mu_0)$ significantly weaker than the gas pressure is Model 3a. There are no acoustic precursors to the Alfvén waves in these models as $v_A > c_s$ everywhere, and indeed the most advanced parts of the density oscillations are not sound waves, but density fluctuations carried by the Alfvén wave at the Alfvén speed. Such a density fluctuation is expected to obey the relationship

$$\frac{\Delta \rho}{\rho} = \frac{v_z}{v_A} \quad (30)$$

(Hollweg 1971, Eq. (15)). At 2500 s this relationship is satisfied for $z > 2.5R_\odot$, but at smaller heights there is a large density excess (Fig. 10). The density enhancement grows in extent with time (Fig. 11). The local maximum is moving outwards at the sound speed, $1.3 \times 10^5 \text{ m s}^{-1}$. All the Models 3 crash eventually, Model 3a and b at the time that they hit the upper boundary, and Model 3c at a much earlier time, when the Alfvén wave evacuates a part of the grid.

3.2 Energetics

As in Paper 1 the equations for the magnetic and kinetic energies are

$$\frac{\partial}{\partial t} \frac{B^2}{2\mu_0} + \nabla \cdot \mathbf{S} = -\frac{\mathbf{J}^2}{\sigma} - \mathbf{v} \cdot (\mathbf{J} \times \mathbf{B}), \quad (31)$$

and

$$\frac{\partial}{\partial t} \left(\frac{1}{2} \rho v^2 \right) + \nabla \cdot \left(\frac{1}{2} \rho v^2 \mathbf{v} \right) = -\mathbf{v} \cdot \nabla \mathbf{p} + \mathbf{v} \cdot (\mathbf{J} \times \mathbf{B}) + \rho \mathbf{v} \cdot \mathbf{g}, \quad (32)$$

where $\mathbf{S} = \mathbf{E} \times \mathbf{B}/\mu_0$ is the Poynting vector, and the electric field is given by $\mathbf{E} = -\mathbf{v} \times \mathbf{B} + \mathbf{J}/\sigma$. The Ohmic dissipation \mathbf{J}^2/σ in Eq. (31) represents the effect of the numerical diffusion in our code. The numerical diffusion smears out discontinuities over the length scale of the grid spacing, but it is at the same time negligible in regions with smooth velocities and magnetic fields. The thickness of a current sheet is proportional to $1/\sigma$, from which it follows that $\mathbf{J} \propto \sigma$, so that the dissipation integrated over the current sheet is independent of σ . The magnitude of the numerical diffusion should thus not affect the net damping unless the diffusion is strong enough to damp out smooth variations, which is not the case. As was pointed out in Paper 1 it is impossible to calculate the Ohmic dissipation directly from the quantities of the numerical simulation, however the other terms in Eq. (31) are accessible. We average these terms over the period of the Alfvén wave. The averages of the nonlinear models are sensitive to secular changes and aperiodic fluctuations in the simulations, which introduce some uncertainties in

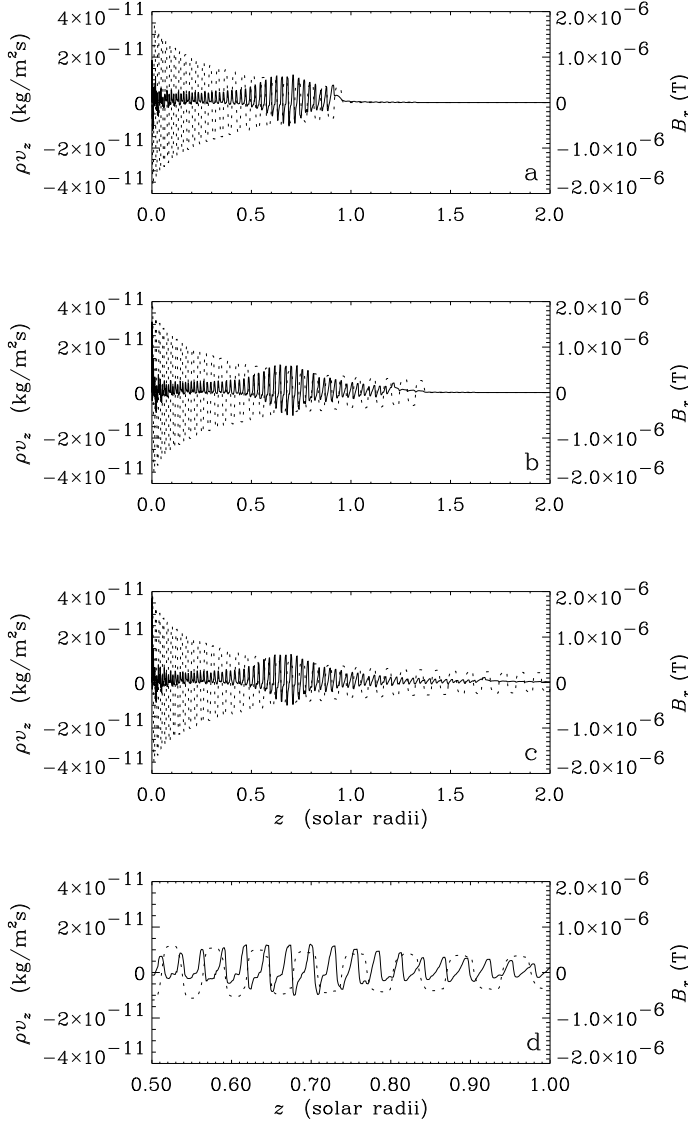


Figure 8. ρv_z (solid line/left scale) and B_x (dotted line/right scale) for the Alfvén wave of Model 2b. (a), (b) and (c) are for the times 7 200, 8 800 and 11 200 s, respectively. (d) Shows an enlargement of the region between $0.5R_\odot$ and $1R_\odot$ in (c). Note how the acoustic oscillation (solid line) increases in amplitude up until $z = 0.7R_\odot$, after which it decreases again, possibly due to dissipation in shocks (d)

the calculated energy losses. We plot the time average of Model 2b as an illustrative example in Fig. 12. 10 - 20 % of the Poynting flux is dissipated immediately at the lower boundary due to imperfections in the boundary conditions and initial state, and it may therefore be advisable to think of the waves as being of correspondingly lower amplitude than indicated from Tab. 1. Most of the remaining Poynting flux is lost between 3 and 5 R_\odot by doing work on the background medium via the Lorentz force. The damping becomes more efficient with increasing amplitude of the Alfvén wave both in the sense that more of the flux is lost from the wave and in the sense that the damping sets in earlier (Tab. 3). In addition a larger part of the Poynting flux is spent on

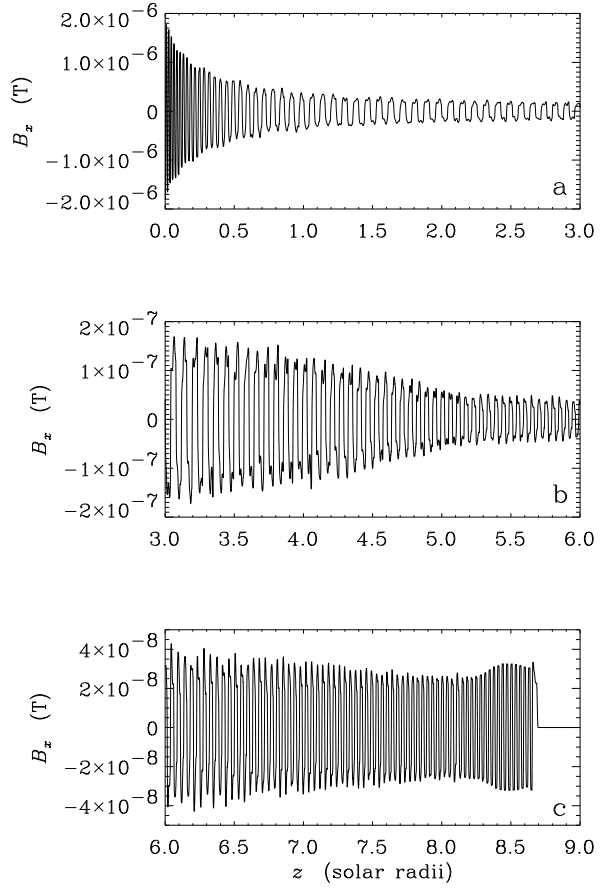


Figure 9. B_x as a function of z for Model 2b at 50 000 s. (a) $0 \leq z \leq 3R_\odot$, (b) $3 \leq z \leq 6R_\odot$ and (c) $6 \leq z \leq 9R_\odot$. The Alfvén wave steepens to a square wave (a), and loses energy in the current sheets (b), but the first few wavelengths in the head are essentially unaffected (c). Below $z = 1R_\odot$, in particular, there are signs of a low-frequency modulation of the Alfvén wave

doing mechanical work instead of being lost through Joule dissipation as the amplitude increases.

4 DISCUSSION

The most important and interesting results from our simulations are

- The fact that practically all our Alfvén waves lose a significant fraction of their Poynting flux within less than 10 R_\odot
- The fact that a nonlinear Alfvén wave can propagate super-Alfvénically
- The appearance of oscillations at lower frequencies than that at which the Alfvén wave is driven

We will discuss each of these facts below, and also the significance of our results for stellar wind models.

4.1 The physical mechanism of the wave damping

It was suggested in Paper 1 that the damping of the Alfvén waves takes place in current sheets. These current sheets ap-

Table 3. A compilation of the energetics of the Alfvén waves. For every Model the Poynting flux is given as the equivalent Poynting flux at the stellar surface, $S_z \left(\frac{R+z}{R} \right)^2$, $S_z(0)$ is the Poynting flux at $z = 0$, and $S_z(\text{final})$ the Poynting flux after the damping of the Alfvén wave. We also give the work done by the wave via the Lorentz force W_{Lor} per unit surface area and time, and the position where half of the damping has taken place, z_{damp}

Model	$S_z(0)$ (W m^{-2})	$S_z(\text{final})$ (W m^{-2})	W_{Lor} (W m^{-2})	z_{damp} (R_\odot)
1a	$4 \cdot 10^{-5}$	$3 \cdot 10^{-5}$	$0.4 \cdot 10^{-5}$	8.2
1b	$4 \cdot 10^{-3}$	$3 \cdot 10^{-3}$	$1 \cdot 10^{-3}$	7.2
1c	$4 \cdot 10^{-1}$	$1 \cdot 10^{-1}$	$3 \cdot 10^{-1}$	1.4
2a	$9 \cdot 10^{-4}$	$0.4 \cdot 10^{-4}$	$4 \cdot 10^{-4}$	9.3
2b	$9 \cdot 10^{-2}$	$0.5 \cdot 10^{-2}$	$4 \cdot 10^{-2}$	4.4
2c	9	.2	9	0.3

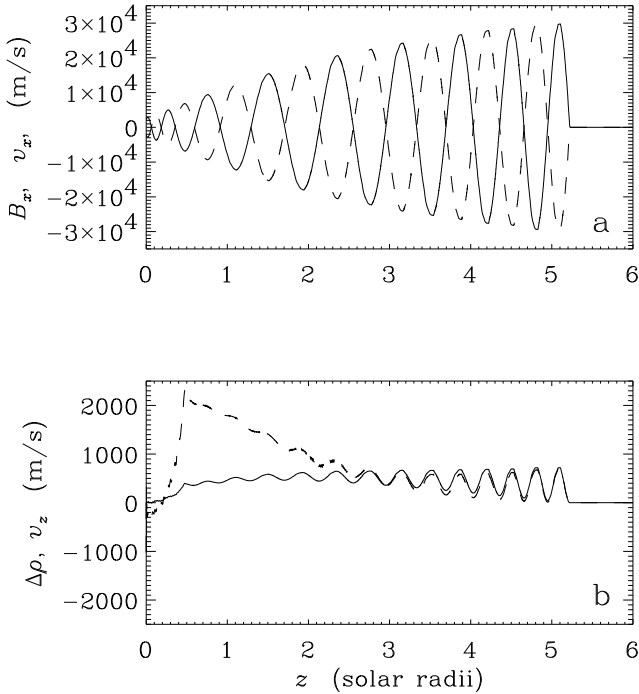


Figure 10. A snapshot of (a) B_x (solid line) and v_x (dashed line), and (b) v_z (solid line) and $\Delta\rho$ (dashed line) at 2500 s for Model 3a. Note that that B_x and $\Delta\rho$ are measured in velocity units by multiplying with $1/\sqrt{\mu_0\rho_0}$ and c_s/ρ_0 , respectively. (a) shows the typical behaviour of an Alfvén wave, while (b) shows density fluctuations carried by the Alfvén wave at $z > 2.5R_\odot$ and an outflow at smaller z

pear at the nodes of the Alfvén wave, because the nodes represent minima of magnetic pressure, and thus oppositely directed magnetic field lines are pushed together at the nodes. This mechanism is still at work in our new simulations, but at the same time, due to the stratification of the medium, there is a gradient in the wave pressure, which in itself may do work on the medium (cf. Jacques 1977). In the nonlinear regime these effects are coupled together and cannot be separated easily. Table 3 shows that the Alfvén wave damping is a nonlinear effect as the fraction of the Poynting flux that is lost increases with increasing initial Poynting flux. In particular it is interesting to find that W_{Lor} increases faster than $S_z(0)$, which we interpret as the transverse magnetic field

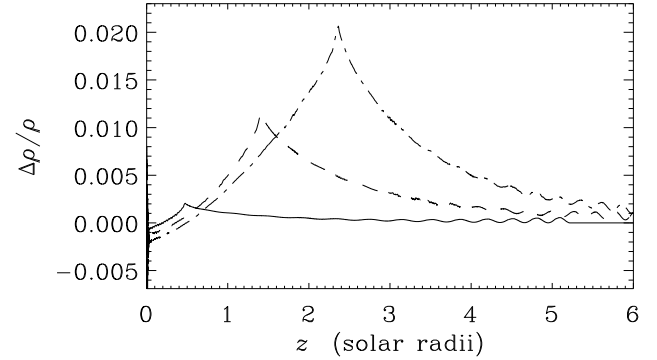


Figure 11. $\Delta\rho/\rho_0$ at 2500 (solid line), 7500 (dashed line) and 12500 s (dot-dashed line) in Model 3a. The peak of $\Delta\rho/\rho$ is moving at the isothermal sound speed

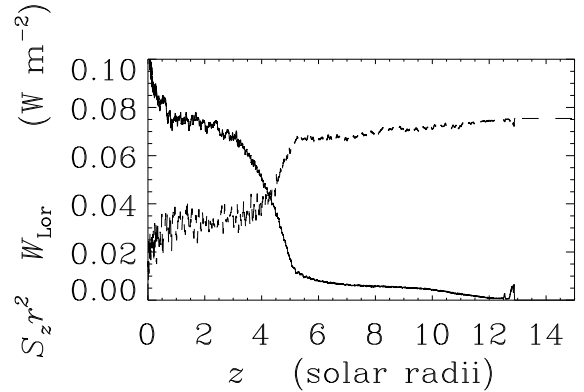


Figure 12. $S_z \left(\frac{R+z}{R} \right)^2$ (solid line) and the integral of the work done by the Lorentz force (dashed line) averaged over 300 s (the period of the Alfvén wave) for Model 2b

becoming more dynamically important compared to the gas pressure. The fact that z_{damp} decreases with $S_z(0)$ shows that the damping cannot be described by a linear model.

4.2 Super-Alfvénic motion

We have seen in some of our simulations that nonlinear Alfvén waves can in some circumstances propagate faster than the local Alfvén speed (Fig. 13a-c). The reason that

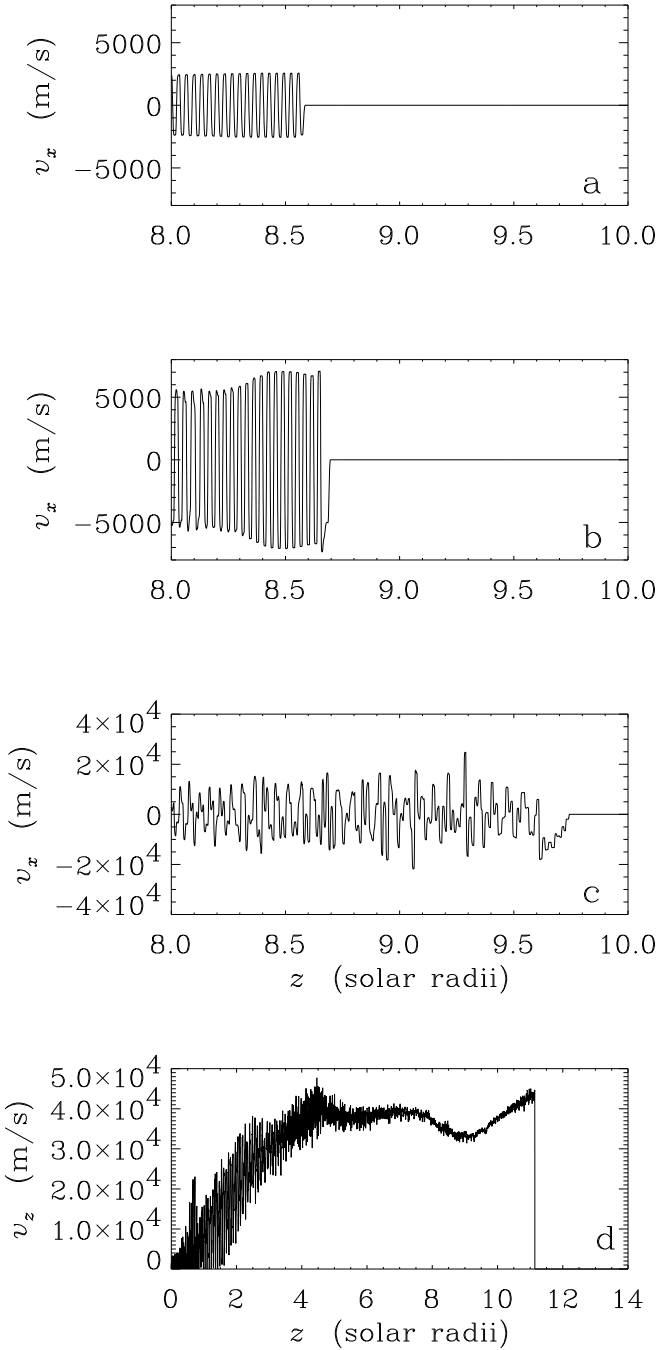


Figure 13. v_x for Models 2a-c at 50 000 s (a - c), and v_z for Model 2c (d). Note the change of v_x -scale between (b) and (c), and the change of z -scale between (c) and (d). This Fig. shows that the wave front propagates faster the higher the amplitude of the wave

the wave in Model 2c can propagate at a higher speed than those in Models 2a and b is that the wave itself is accelerating an outflow with a maximum velocity of $4.8 \times 10^4 \text{ m s}^{-1}$ (Fig. 13d). Thus the Alfvén wave gains the velocity of the medium it is propagating in. This effect was not found in Paper 1, as in the plane-parallel models the Alfvén velocity is increasing upwards to eventually become supersonic. Con-

sequently the Alfvén wave front manages to stay in front of the main outflow (cf. Paper 1, Fig. 7), which is generated by the nonlinear part of the wave at lower altitudes.

4.3 Low-frequency modulations

As already noticed there is some evidence in Fig. 9 that the Alfvén wave is modulated on a frequency lower than the driving frequency. To test this we calculate power spectra of Models 1b and 2b (Fig. 14). In addition to the main peak at 0.003 2 Hz we see side peaks at 0.003 0 and 0.000 6 Hz. To explain these extra peaks we note that a wave reflected back down by an inhomogeneity propagating upwards is Doppler-shifted to a lower frequency

$$\nu = \nu(0) \frac{v_A - v_z}{v_A + v_z}, \quad (33)$$

where $\nu(0)$ is the original frequency of the wave. To explain the side peak in Model 1b we require an outflow velocity $v_z = 0.04v_A$, which agrees well with the velocities generated in the model (Fig. 14b). The peak at 0.000 6 Hz of Model 2b on the other hand requires $v_z = 0.7v_A$, which is significantly higher than what is available (Fig. 14d). An alternative interpretation in this case is that the frequency 0.000 6 Hz represents the beat frequency between the original and reflected Alfvén waves, thus giving the frequency of the reflected Alfvén wave as 0.002 6 Hz, corresponding to $v_z = 0.1v_A$. This agrees well with the velocity before the jump in v_z at $11 R_\odot$ (Fig. 14d), but the peak in the power spectrum (Fig. 14c) is at 0.002 Hz, which may be a consequence of the inhomogeneity of the medium.

4.4 Importance for stellar winds

Alfvén-wave driven winds have been discussed several times in the past (e.g. Hartmann & MacGregor 1980, 1982; Leer et al. 1982, MacGregor & Charbonneau 1994). The main reason is that the Alfvén waves may be able to drive the wind in circumstances where more well-understood mechanisms can be shown to be insufficient. This is for instance the case for the fast solar wind moving at velocities of 800 km s^{-1} , which is too fast for the classical thermally driven wind model by Parker (1958), and the winds of late-type giants, where the temperatures are too low to drive a wind. A severe weakness of the models of the winds of late-type stars is that the Alfvén waves must be damped within a few stellar radii in order to avoid over-accelerating the wind. Usually this has been done by ascribing an arbitrary damping length to the Alfvén waves, but the resulting models are sensitive to the choice of the damping length (Holzer et al. 1983). In our simulations the waves are damped without the action of any dissipative mechanism while they are doing work on the background medium. Our mechanism does not require the wavelength to become comparable to the length scale of the Alfvén velocity variations in contrast to some previous attempts that have appealed to non-WKB waves being reflected. Although we have not surveyed the parameter space it appears likely that the parameters of our model can be modified to provide a sufficiently effective damping to fulfill the constraints put on those wind models. An obvious improvement on our current simulations is to start from an initial state which describes an outflowing wind.

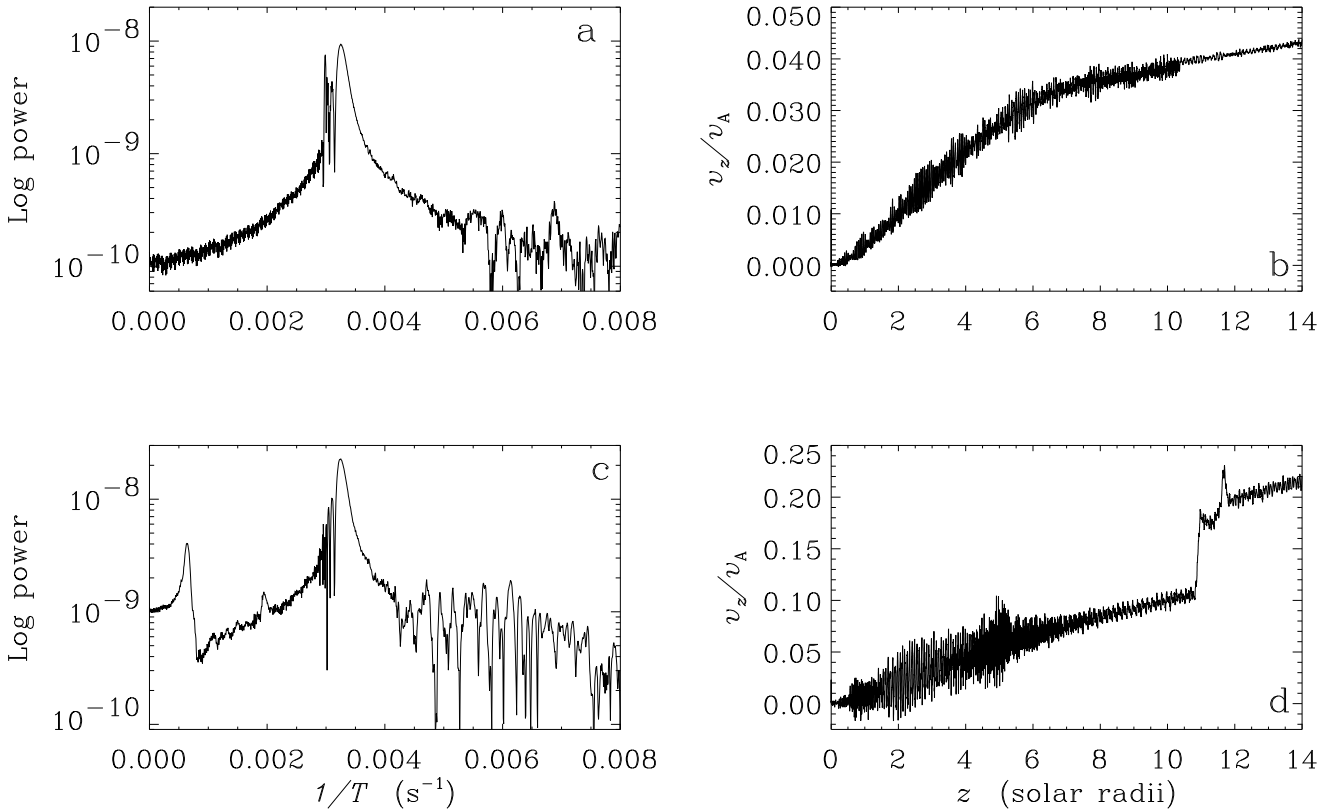


Figure 14. Power spectra of B_x for Models 1b (a) and 2b (c) at $t = 100\,000$ s. (b) and (d) show v_z in units of the local Alfvén velocity at the same time for Models 1b and 2b, respectively

Magnetohydrodynamic waves may have been observed in the inner parts of the solar wind. Ofman & Davila (1997b) have calculated that magnetohydrodynamic waves in the solar wind may give a line broadening of $\sim 300 \text{ km s}^{-1}$, which is comparable to the line widths observed by *SOHO* (e.g. Kohl et al. 1996). In particular Ofman & Davila (1997a) suggests that what they call *solitary* waves are essential for the acceleration of the solar wind. The solitary waves are propagating ρv_z -perturbations generated by Alfvén waves, and thus are akin to the density oscillations we have found in for instance Fig. 8. The authors call them solitary waves as they believe them to be related to the solitary wave solutions found in slabs and thin flux tubes by Roberts (1981) and Roberts & Mangeney (1982). This is an interpretation that we find questionable for the following reason. It is certainly true that the two-dimensional axisymmetric model used by Ofman & Davila bears some resemblance to a flux tube with a lower density in the interior, but our one-dimensional simulations lack all features characteristic of a flux tube, and still we find the same kind of density oscillations propagating faster than the sound speed. We thus conclude that the oscillations cannot be related to the existence of solitons in flux tubes. Regarding the question of whether the solar wind is driven by Alfvén waves or *solitary* waves that is very much a matter of semantics as the *solitary* waves must be driven by the Alfvén waves. It is interesting to compare the simulations in terms of efficiency of deriving energy from the

Alfvén waves. The background models are roughly similar apart from that Ofman & Davila assume a radial magnetic field which is 70% stronger than the one we use in Models 3. They drive the Alfvén wave at an amplitude inbetween our Models 3a and b, and assume a period which is almost an order of magnitude longer than ours. Consequently they find larger radial velocities than we do, but unfortunately they do not give any numbers for the fraction of the Poynting flux that has been converted to mechanical energy. They do however state that $3 \cdot 10^{-3}$ of the Poynting flux has been lost due to Ohmic dissipation. This appears to be a rather inefficient conversion process, but one must keep in mind that their grid extends only to $4 R_\odot$, and we typically find that most of the damping takes place at larger distances.

Naturally there are alternative models for driving the fast solar wind. Feldman et al. (1996) have suggested that the outflows are driven by the same kind of reconnection events that produce the X-ray jets (Yokoyama & Shibata 1995). In this model the emerging magnetic field of a bipolar region collides with the magnetic field of the chromospheric network. This field is concentrated in narrow flux tubes in the photosphere, but due to the stratification the flux tube increases in radius upwards. At the collision point the magnetic fields reconnect and two jets moving at close to the Alfvén velocity appear. Only a part of the momentum of the jet is directed upwards, but the horizontal momentum is absorbed by nearby matter and magnetic field, so that also

a part of this becomes available for generating an outflow from the coronal hole. Inevitably some of the energy goes into producing Alfvén waves, and so the model may also explain the presence of Alfvén waves in the solar wind.

5 CONCLUSIONS

In this paper we have studied the propagation of nonlinear spherical Alfvén waves. Like in our previous simulations of Alfvén waves in a plane-parallel atmosphere the waves damp by forming current sheets in which Poynting flux is lost to Ohmic heating and the acceleration of an outflow. In general most of the Poynting flux is spent on accelerating an outflow. This combined process of damping Alfvén waves and accelerating an outflow may be important in understanding both the fast solar wind and the winds of late-type giants.

ACKNOWLEDGEMENTS

Our work on nonlinear Alfvén waves was begun as part of a collaborative research project between the Astronomical Institute, Utrecht, and the FOM Institute for Plasma Physics, Rijnhuizen, the Netherlands. We are grateful to the other members of this collaboration, J. P. Goedbloed, A. G. Hearn, S. Poedts and G. Tóth for a stimulating environment. UT is supported by an EU post-doctoral fellowship. We thank G. Ogilvie for reading the manuscript and providing useful comments, and J. Orta for spotting an error in our code. Finally we thank an anonymous referee for helpful comments.

REFERENCES

- An, C.-H., et al., 1990, *ApJ*, 350, 309
 Balogh A., et al., 1995, *Sci*, 268, 1007
 Belcher, J. W., Davis Jr., L., 1971, *J. Geophys. Res.*, 76, 3534
 Bohlin, J. D., 1976, in D. J. Williams (ed.) *Physics of solar planetary environments*, American Geophysical Union, 114
 Boynton G. C., Torkelsson U., 1996, *A&A*, 308, 299 (Paper 1)
 Feldman, W. C., et al., 1996, *A&A*, 316, 355
 Hartmann, L., MacGregor, K. B., 1980, *ApJ*, 242, 260
 Hartmann, L., MacGregor, K. B., 1982, *ApJ*, 257, 264
 Heinemann, M., Olbert, S., 1980, *J. Geophys. Res.*, 85, 1311
 Hollweg, J. V., 1971, *J. Geophys. Res.*, 76, 5155
 Holzer, T. E., Flå, T., Leer, E., 1983, *ApJ*, 275, 808
 Jacques, S. A., 1977, *ApJ*, 215, 942
 Kohl, J. L., et al., 1996, *BAAS*, 28, 897
 Lamb, H., 1908, *Proc. Lond. Math. Soc.*, (2), VII, 122
 Lamb, H., 1932, *Hydrodynamics*, Cambridge University Press, Cambridge
 Landau, L. D., Lifshitz, E. M., 1987, *Fluid Mechanics*, Pergamon Press, Oxford
 Leer, E., Holzer, T. E., Flå, T., 1982, *Space Sci. Rev.*, 33, 161
 Lou, Y.-Q., Rosner, R., 1994, *ApJ*, 424, 429
 MacGregor, K. B., Charbonneau, P., 1994, *ApJ*, 430, 387
 Ofman, L., Davila, J. M., 1997a, *ApJ*, 476, 357
 Ofman, L., Davila, J. M., 1997b, *ApJ*, 476, L51
 Parker, E. N., 1958, *ApJ*, 128, 664
 Roberts, B., 1981, *Solar Phys.*, 69, 39
 Roberts, B., Mangeney, A., 1982, *MNRAS*, 198, 7P
 Yokoyama, T., Shibata, K., 1995, *Nat*, 375, 42
 Zirker, J. B., 1977, *Coronal holes and high speed wind streams*, Colorado University Press, Boulder